Chemistry & Biology
Article

Heterotaxin: A TGF-β Signaling Inhibitor Identified in a Multi-Phenotype Profiling Screen in *Xenopus* Embryos

Michael K. Dush,[1] Andrew L. McIver,[2] Meredith A. Parr,[1] Douglas D. Young,[2] Julie Fisher,[3] Donna R. Newman,[1] Philip L. Sannes,[1] Marlene L. Hauck,[3] Alexander Deiters,[2,*] and Nanette Nascone-Yoder[1,*]
[1]Department of Molecular Biomedical Sciences, College of Veterinary Medicine
[2]Department of Chemistry
[3]Department of Clinical Sciences, College of Veterinary Medicine
North Carolina State University, 4700 Hillsborough Street, Raleigh, NC 27606, USA
*Correspondence: alex_deiters@ncsu.edu (A.D.), nanette_nascone-yoder@ncsu.edu (N.N.-Y.)
DOI 10.1016/j.chembiol.2010.12.008

SUMMARY

Disruptions of anatomical left-right asymmetry result in life-threatening heterotaxic birth defects in vital organs. We performed a small molecule screen for left-right asymmetry phenotypes in *Xenopus* embryos and discovered a pyridine analog, heterotaxin, which disrupts both cardiovascular and digestive organ laterality and inhibits TGF-β-dependent left-right asymmetric gene expression. Heterotaxin analogs also perturb vascular development, melanogenesis, cell migration, and adhesion, and indirectly inhibit the phosphorylation of an intracellular mediator of TGF-β signaling. This combined phenotypic profile identifies these compounds as a class of TGF-β signaling inhibitors. Notably, heterotaxin analogs also possess highly desirable antitumor properties, inhibiting epithelial-mesenchymal transition, angiogenesis, and tumor cell proliferation in mammalian systems. Our results suggest that assessing multiple organ, tissue, cellular, and molecular parameters in a whole organism context is a valuable strategy for identifying the mechanism of action of bioactive compounds.

INTRODUCTION

Vertebrate embryos develop with left-right asymmetry, evident in the asymmetric anatomical positioning of the heart and other vital organs. Correct asymmetries are essential for the function of the cardiovascular and digestive systems, and severe malformations are linked to disruptions of organ laterality. Complete reversal of normal left-right asymmetries (*situs inversus*) occurs in one in 8,500 births (Brueckner, 2007), whereas "heterotaxia," in which one or more organs deviate from normal by appearing independently and randomly oriented with respect to left and right, occurs in one in 10,000 births (Brueckner, 2007). Heterotaxia is often accompanied by intracardiac defects and is associated with at least 3% of all congenital heart disease (Zhu et al., 2006). Also associated with heterotaxia is intestinal malrotation, which occurs in as many as one in 500 births and predisposes affected individuals to life-threatening conditions (Kamal, 2000).

The initial establishment of the left-right axis eventually results in the expression of genes exclusively on the left side of the embryo, including the TGF-β family members *nodal* and *lefty*, and the transcription factor *Pitx2* (Levin, 2005). Although it has been demonstrated that *situs inversus* or heterotaxia can result if these genes are misexpressed, how such left-right cues are translated into the asymmetric morphology of developing organs is poorly understood. Such knowledge is essential for understanding the etiology of congenital deformities.

In recent years, whole organism chemical-genetic strategies, in which pharmacologically well-characterized small molecules are screened in living embryos for their ability to induce a developmental phenotype of interest, have been successfully used to illuminate the mechanisms that establish the initial left-right axis of the early embryo (e.g., Adams et al., 2006). However, the efficacy of such screening strategies is limited by the availability of known bioactives capable of exerting specific effects on developing model organisms. To our knowledge, no discovery-based screens have been employed to uncover novel compounds that perturb left-right asymmetric organ morphogenesis. Identifying novel heterotaxia-inducing small molecules may not only offer an increased understanding of the molecular etiology of common birth defects but may also reveal new classes of small molecules capable of modulating pathways that play important roles in development and disease.

Unfortunately, uncovering the mechanism of action of a novel molecule identified in a whole organism or phenotype-based screen remains a major challenge. Increasingly, multiparameter phenotypic profiling is being used to categorize small molecules discovered in high-throughput biochemical assays or cell-based screens, providing insight into mechanism of action by similarities to reference compounds with known cellular targets (Feng et al., 2009). However, even compounds identified in multiplex strategies may still be ineffectual or have unpredictable or toxic effects in vivo.

Here, we describe an approach to small molecule discovery that combines the advantages of whole organism screening and multiplex profiling by generating a multiparameter profile

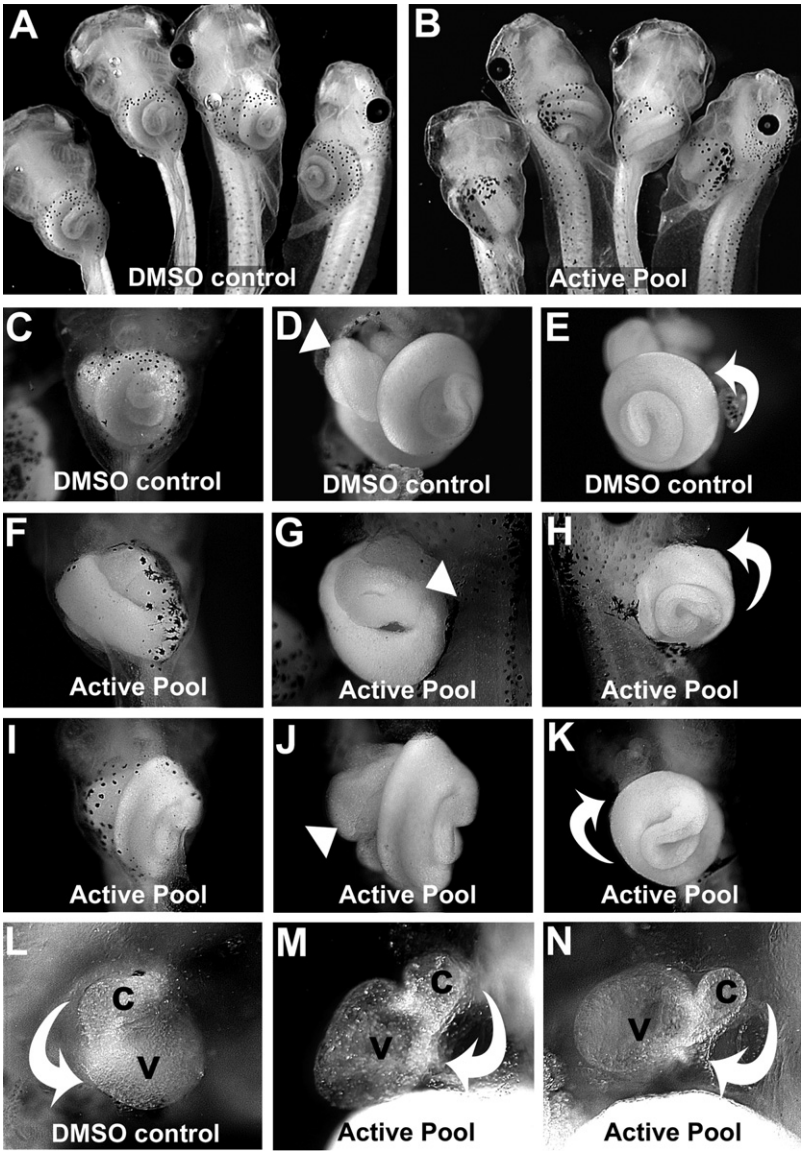

Figure 1. A Mixture of Pyridine Regioisomers Causes Heterotaxia in *Xenopus*

Embryos were treated with (A) DMSO or (B) 200 μM active pool. (C) Ventral view of organs in intact DMSO control tadpole. Ventral (D) and left-ventral (E) views of tadpole in (C) with skin removed, showing the normal asymmetry (arrowhead, D) of the foregut loop, and the normal counterclockwise rotation of the intestine (curved arrow, E). (F) Tadpole exposed to active pool. Ventral (G) and right-ventral (H) view of tadpole in (F) with skin removed, showing the reversed position (arrowhead, G) of the foregut loop. The intestine is coiling in the normal direction (curved arrow, H) but is located on the opposite side of the animal. Ventral views of tadpole exposed to active pool (I–K) show normal foregut looping (arrowhead, J) but the intestine coiling in the reversed direction (i.e., clockwise; curved arrow, K). (L) Ventral view of heart of DMSO control, with outflow tract (conus, c) and ventricle (v) indicated, with the normal direction of cardiac looping (curved arrow). (M and N) Two examples of heterotaxin-induced reversed heart looping (curved arrows).

of embryonic phenotypes. Recent studies have illustrated the promise of embryos of the aquatic frog, *Xenopus laevis*, for small molecule discovery (e.g., Tomlinson et al., 2009). A unique feature of *Xenopus* embryos, not found in other models (e.g., zebrafish), is the morphogenesis of their left-right asymmetric organs, which is highly analogous to humans and easily visible in situ (Muller et al., 2003). Therefore, we employed *Xenopus* embryos in a screen for heterotaxia-inducing compounds and identified a novel pyridine-based molecule, which we named "heterotaxin." Further analyses of the in vivo phenotypic profile of this compound revealed that it elicits multiple TGF-β-dependent phenotypes throughout development and inhibits TGF-β-dependent intracellular signaling events, identifying it as a new TGF-β signaling inhibitor. Importantly, heterotaxin analogs also disrupt invasive phenotypes, angiogenesis, and tumor cell proliferation in mammalian systems, revealing a new class of compounds with TGF-β-inhibitory therapeutic potential.

RESULTS

The Discovery of Heterotaxin (1)

A solid-supported multicomponent cyclotrimerization reaction (Young et al., 2007) was utilized to generate a pilot library of ~130 novel compounds as 44 pools of regioisomers. We arrayed *X. laevis* embryos in individual wells of a 24-well plate in growth media supplemented with pools of regioisomers (200 μM). After the embryos had completed asymmetric morphogenesis, the morphology of the heart and digestive tract was assessed in anesthetized tadpoles. All controls, i.e., untreated or exposed to DMSO alone, had normal organ asymmetries (Figures 1A, 1C–1E, and 1L), as did the embryos in 33/44 (75%) pools. In our initial screen, 2/44 pools (4.5%) were lethal at 200 μM, and 8/44 pools (18%) elicited multiple defects (in organ, eye, craniofacial and tail development) in exposed embryos. However, one pyridine pool induced clear heterotaxia (heart and/or gut looping defects) in 100% of the exposed individuals (Figures 1B, 1F–1K, 1M, and 1N). In three repeat trials with embryos derived from oocytes obtained from different mothers, this pool was effective at inducing heterotaxia in at least 50% of embryos exposed at a concentration of 100–200 μM. Overall, 89% (n = 28) of the embryos in all trials that were exposed to the active regioisomer pool at 100–200 μM exhibited heterotaxia phenotypes, strongly implicating one or more regioisomers in this pool as an inhibitor of a cellular target(s) required for normal left-right asymmetric organ development.

Identification of the Active Heterotaxia-Inducing Regioisomer

To facilitate the isolation of the regioisomer responsible for the observed heterotaxia phenotypes, the solid-phase synthesis used to generate the original pool was conducted on a 5-fold

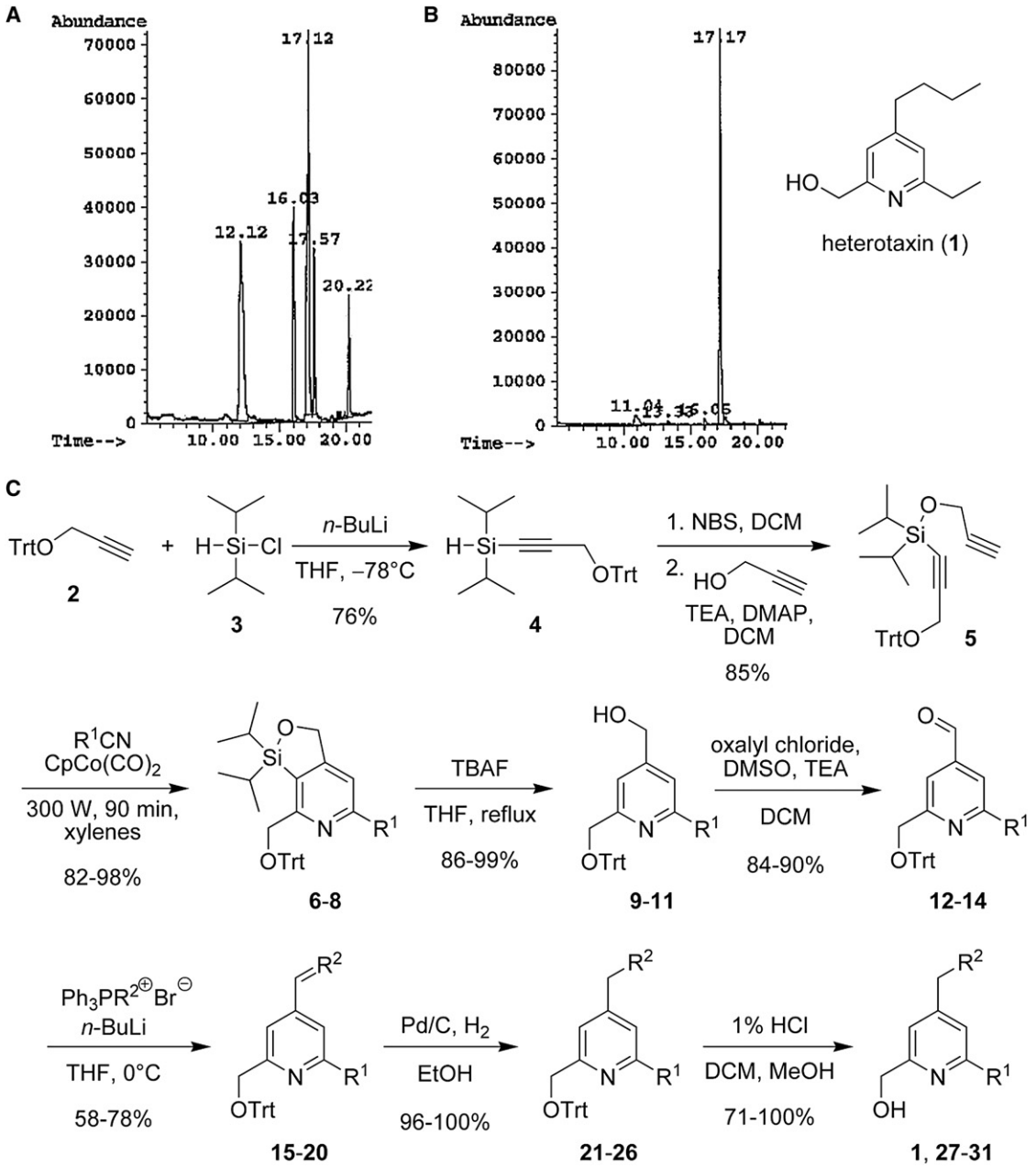

Figure 2. Purification, Identification, and Synthesis of Heterotaxin (1)

(A) GC trace of the regioisomers in the active pool.

(B) Active regioisomer (**1**) after separation (see Supplemental Experimental Procedures), phenotypic assay, and structural assignment.

(C) Regioselective synthetic route toward gram quantities of heterotaxin (**1**) and analogs (**27–31**).

larger scale. A GC trace of the heterotaxia-inducing pool prior to purification indicated the presence of several different regioisomers (Figure 2A). After separating these components by flash-column chromatography on silica gel, we found that only the 2,4,6-regioisomer **1** (Figure 2B; GC retention time of 17.17 min) displayed the ability to induce the desired phenotype in *Xenopus* embryos (data not shown).

As further confirmation, we exposed embryos of a related species, *Xenopus tropicalis*, to this purified component. Despite the differences between the *X. laevis* and *X. tropicalis* species in culture temperature (15°C versus 24°C, respectively), size (1.2 versus 0.7 mm, respectively), and growth rate (7–8 versus 3–4 days, respectively), the regioisomerically pure compound induced identical heterotaxic organ deformities in both the heart and gut as observed in *X. laevis* (data not shown). Due to its "heterotaxia-inducing" propensity, we named the purified, active regioisomer "heterotaxin."

A Regioselective Synthetic Route to Heterotaxin

Our original synthesis route toward heterotaxin necessitated laborious purification of the 2,4,6-regioisomer **1** from a mixed pool and was, therefore, inefficient for generating the large (milligram) quantities of heterotaxin required for further characterization. Consequently, we developed a robust, scalable synthetic approach to heterotaxin, with a sequence of chemical transformations that provided a completely regioselective synthesis (Figure 2C).

The synthesis commenced with the condensation of the lithiated trityl-protected propargyl alcohol **2** and commercially available chlorodiisopropylsilane (**3**) to afford the silane **4** in 76% yield (Petit et al., 2003). The silane **4** was then subjected to in situ bromination by NBS, followed by a subsequent reaction with propargyl alcohol in the presence of TEA and DMAP in DCM to afford the silyl ether **5** in 85% over two steps (Petit et al., 2003). The key step of the synthesis was a microwave-mediated, cobalt-catalyzed [2+2+2] cyclotrimerization reaction between the diyne **5** and propionitrile under open-vessel conditions. This delivered the pyridine **6** in 98% yield. The silicon tether allowed for a completely regioselective pyridine formation (Bols and Skrydstrup, 1995), with the C-N bond being formed with the substituted *sp*-carbon center bearing the CH_2OTrt group. The silicon tether was then removed using TBAF in refluxing THF to afford the regioisomerically pure 2,4,6-substituted pyridine **9** in 99% yield. The alcohol **9** was converted into the aldehyde **12** in 90% yield using a Swern oxidation. Following the oxidation, a Wittig reaction was employed to install the C_4 chain at the 4-position affording the alkene **15** in a moderate yield of 78%. Reduction of the double bond in **15** with Pd/C under 1 atm of H_2 furnished the pyridine **21** in almost quantitative yield. The acid-catalyzed deprotection of the trityl group proceeded smoothly and delivered heterotaxin (**1**) in 100% yield. This schematic route allowed us to synthesize reasonable (37 mg) quantities of heterotaxin, and analogs thereof (see below), which we used to further investigate the mechanism by which it induces heterotaxia, and to elucidate its mechanism of action.

Multiple Phenotypes Are Induced by Heterotaxin

Heterotaxin perturbs organ laterality, suggesting that it interferes with global embryonic left-right patterning. Indeed, heterotaxin perturbs left-right asymmetric gene expression patterns in the lateral plate mesoderm (LPM). For example, in heterotaxin-treated embryos, the pattern of the *Xenopus nodal* homolog, *Xnr-1*, is randomized with respect to left and right (Figures 3A–3D). Although some embryos exhibit normal left-side *nodal* expression (36%, n = 28), some show bilateral *nodal* expression on both the left and right sides (18%, n = 28), some exhibit reversed (i.e., right-sided) *nodal* expression (11%, n = 28), and some (36%, n = 28) completely lack *nodal* expression on either side (Figure 3I). As expected, the expression patterns of the *Xenopus* homolog of *Pitx2*, a transcription factor whose expression is dependent on *nodal* activity, is similarly randomized by exposure to heterotaxin (Figures 3E–3H and 3J). These results confirm that the organ anomalies induced by heterotaxin represent bona fide left-right asymmetry defects.

To gain further information about heterotaxin's mechanism of action, we carefully assessed heterotaxin-treated embryos throughout development (Figure 4). Compared to DMSO-treated controls (Figure 4A), the melanocytes in heterotaxin-treated tadpoles exhibit a striking increase in pigmentation and dendricity (Figures 4B and 4C), and the number of melanocytes is reduced by as much as 50% (Figure 4D). Exposure to heterotaxin also results in dilated vitelline vessels and ventral hemorrhaging (Figures 4E–4G), suggesting that the compound perturbs the normal processes of vasculogenesis and/or angiogenesis.

Finally, in addition to being malrotated, the digestive tracts of embryos exposed to heterotaxin are wider and shorter than controls (e.g., see Figures 4E and 4G). The elongation of the digestive tract is driven by the rearrangements of endoderm cells within the embryonic gut tube, a process that also facilitates the formation of the gut lumen and epithelial lining (Reed et al., 2009). The endoderm cells are initially round but adopt an elongated shape and remodel their intercellular adhesive junctions as they move toward the circumference of the gut, intercalating between each other to form a single layer (Reed et al., 2009). In controls the resultant simple columnar epithelium can be observed lining the lumen of the lengthened coils of gut (arrows, Figure 4H). In contrast, in heterotaxin-treated embryos, the digestive epithelium is still stratified and contains clumps of rounded cells that have failed to rearrange into a single layer (arrows, Figures 4I and 4J). These dysmorphic cells block the gut lumen and exhibit increased intercellular adhesion, as indicated by their intensified E-cadherin staining (arrows and inset, Figures 4I and 4J). This unusual morphology suggests that the normal acquisition or maintenance of migratory cell properties in the embryonic endoderm is inhibited in these embryos, preventing the cell rearrangements required for normal gut elongation.

Identifying the Phenocritical Period for the Effects of Heterotaxin

To determine the phenocritical period in which heterotaxin elicits each of the above phenotypes, we exposed embryos to heterotaxin for limited times (Figure 4K). The expression of left-right genes in the *Xenopus* embryo peaks between stages 19 and 26 (Ohi and Wright, 2007). To determine whether heterotaxin directly affects left-right gene expression or function, we exposed embryos to heterotaxin at successively later stages of development beginning at stage 12 (gastrula), 18 (neurula), 26 (late neurula), or 32 (tailbud). The compound can elicit robust heterotaxic organ phenotypes when applied as late as stage 18, but will induce heterotaxia only at low frequency at stage 26, and has no effect on organ asymmetry when applied at stage 32 (Figure 4K). We then exposed embryos to heterotaxin through stage 26, washed away the compound with multiple rinses in fresh media, and cultured in the absence of heterotaxin through organogenesis. We found that even this limited exposure can disrupt organ asymmetries (Figure 4K), suggesting that heterotaxin affects left-right asymmetry between stages 18 and 26, coinciding with the peak of left-right gene expression.

We used similar exposures to determine the period in which heterotaxin induces other phenotypes. The melanogenesis phenotype can be elicited even when heterotaxin is applied as late as stage 32 (Figure 4K), suggesting that the compound acts directly on developing melanocyte precursors, which migrate and differentiate between stage 30 and 40 (Collazo et al., 1993). Likewise, the effect on gut elongation can also be

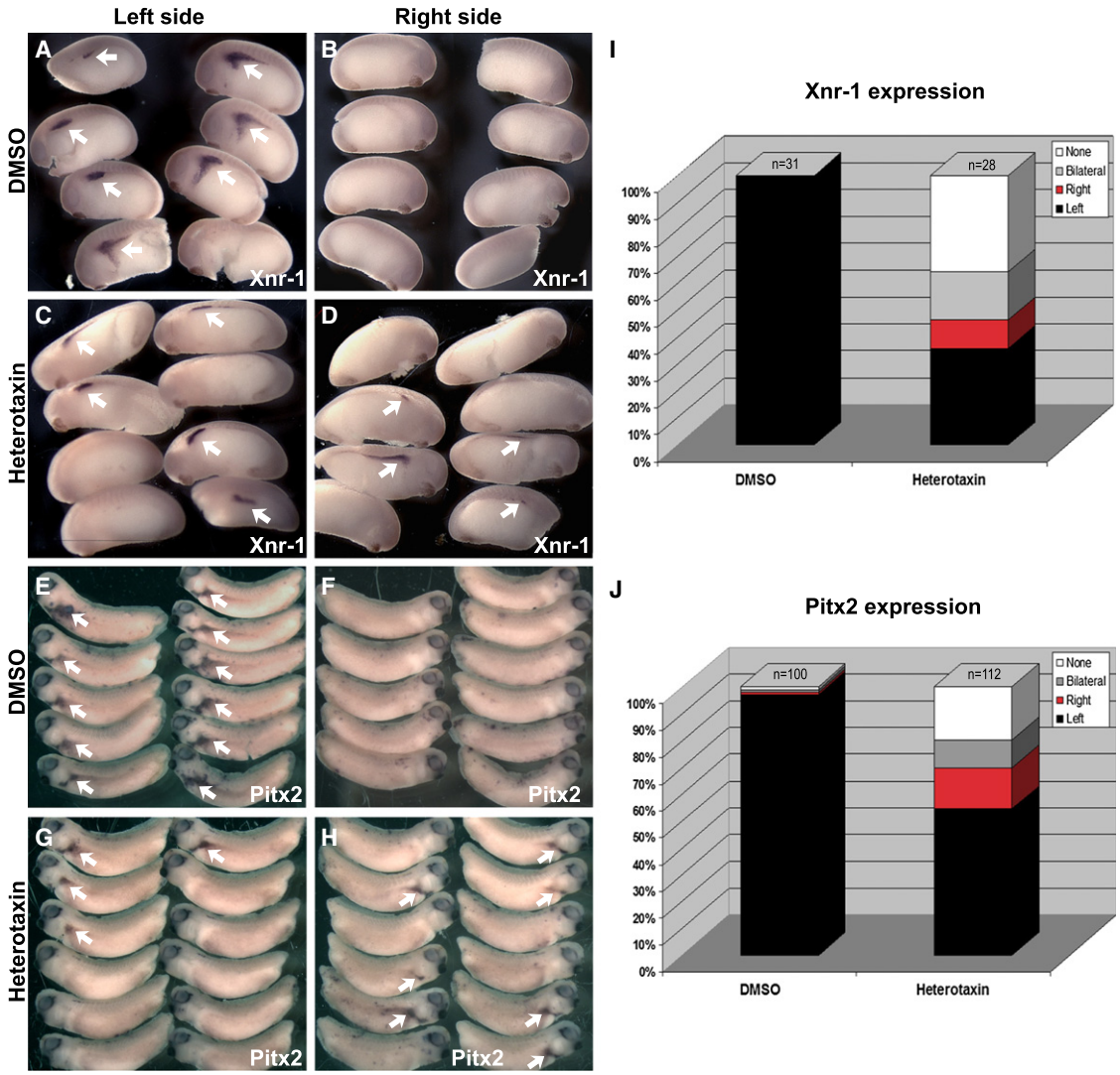

Figure 3. Heterotaxin Perturbs Left-Right Asymmetric Gene Expression Patterns

(A–H) In situ hybridization for *nodal* (*Xnr-1*; A–D), and *Pitx2* (*XPitx2*; E–H) genes was performed on DMSO- (A, B, E, and F) and heterotaxin-treated (C, D, G, and H) embryos. The expression pattern (arrows) is shown for both the left (A, C, E, and G) and right (B, D, F, and H) sides of the embryo (A–D, stage 23; E–H, stage 26). The frequency of embryos exhibiting left only (Left, black), right only (Right, red), bilateral (gray), or absent (None, white) expression of *nodal* (I) or *Pitx2* (J) is quantified in the bar graphs.

elicited by exposure to the compound as late as stage 32 (Figure 4K), just prior to when migratory properties are acquired by endoderm cells in the embryonic gut (Reed et al., 2009), indicating that heterotaxin exerts a direct effect on these cells. In contrast the frequency of heterotaxin-induced vasculogenesis/angiogenesis defects declines at stage 32 (Figure 4K). Because the genes that regulate the formation of the vitelline veins are expressed between stage 18 and 28 (Walmsley et al., 2002), and the vascular vitelline network is already forming at stage 30 (Inui and Asashima, 2006), the observed window of susceptibility to heterotaxin is consistent with the timing of neovascularization. Overall, these results suggest that multiple independent phenotypes in heterologous tissues result from heterotaxin acting directly and specifically on discrete populations of embryonic cells at different stages of development.

Structure-Activity Relationship Studies of Heterotaxin

To further explore heterotaxin's multifunctionality, we conducted SAR studies with heterotaxin analogs. Our regioselective route to heterotaxin (Figure 2C) was purposely designed in a flexible fashion to enable the introduction of other substituents on the pyridine ring through the selective replacement of the butyl and the ethyl side chain with additional functional groups. This enabled the assembly of a small set of analogs from a common intermediate. The R^1 and R^2 groups were selected as methyl, ethyl, propyl, phenyl, and hydroxymethylene, based on the original side chains found in heterotaxin and in order to probe the size of the putative cellular protein-binding pocket. Thus, we synthesized substantial quantities of the diyne **5** and used that to branch out to the synthesis of analogs. The key step was again a cobalt-catalyzed [2+2+2] cyclotrimerization reaction between

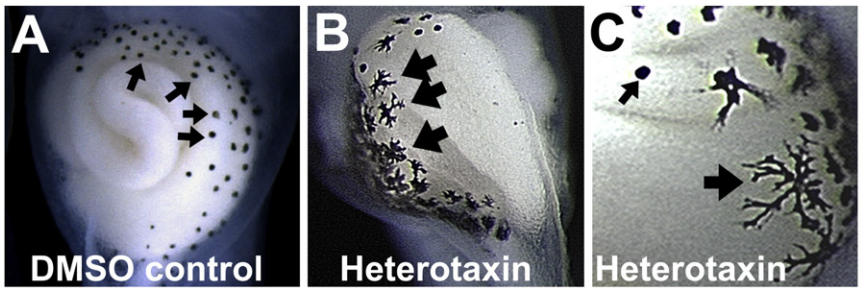

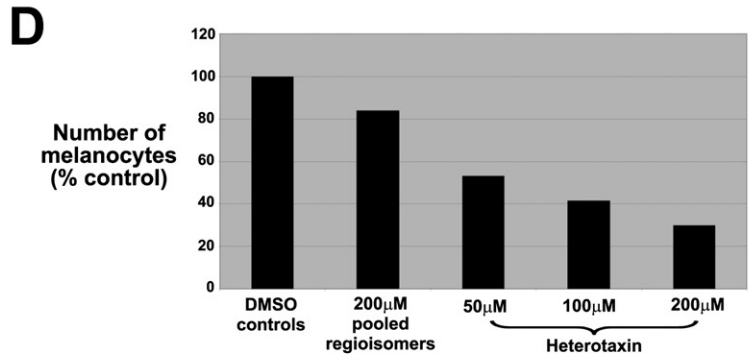

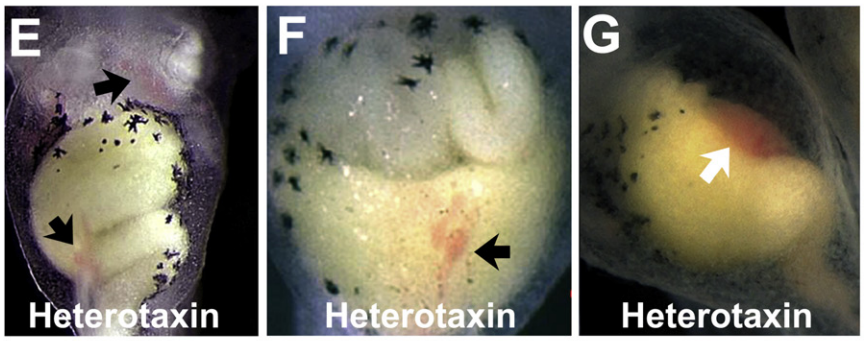

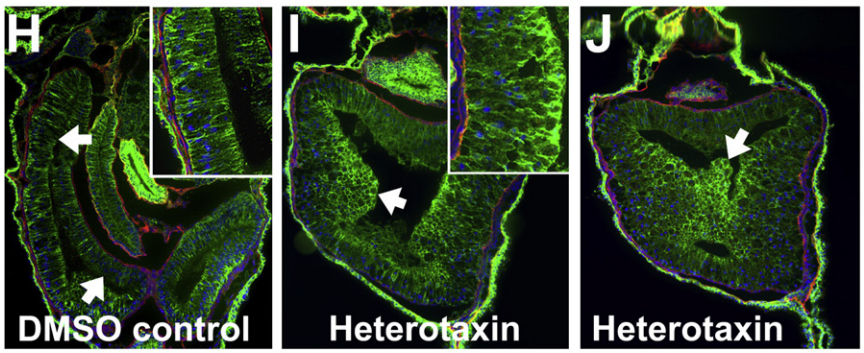

Figure 4. Heterotaxin Perturbs Melanogenesis, Angiogenesis, and Cell Rearrangements

Compared to the round melanocytes seen in DMSO controls (small arrows, A and C), heterotaxin-treated embryos (two different embryos are shown in B and C) exhibit highly dendritic pigment cells (large arrows, B and C).

(D) Number of abdominal melanocytes in embryos exposed to either DMSO, the active pool identified in the original pilot screen, or different concentrations of purified heterotaxin.

(E–G) Heterotaxin induces mild (arrows, E and F) to severe (arrow, G) defects in vasculogenesis (compare the three different examples in E–G to DMSO control in A).

(H–J) Immunohistochemical staining for E-cadherin (green), laminin (red), and nuclei (blue; DAPI) on frontal sections (100×) through the gut tube of embryos treated with DMSO (H, control), 100 μM heterotaxin (I), or 200 μM heterotaxin (J). A single-layer columnar epithelium lines the digestive tract of the DMSO tadpole (arrows, H; inset at 400×), whereas the cells lining the heterotaxin-treated gut are round, exhibit high levels of E-cadherin (green), and have failed to rearrange into a single layer (arrows, I [inset at 400×], J).

(K) Time course studies reveal the sensitivity of each phenotype to heterotaxin exposure. Left-right asymmetry, reversal of heart looping, foregut looping, and/or intestinal rotation; Vasculogenesis/Angiogenesis, hemorrhaging or enlarged blood vessels; Melanogenesis, decreased number and increased dendricity of melanocytes; Migration, perturbed cell rearrangement, indicated by shortening of the primitive gut tube. "+" indicates that at least 75% of embryos exhibited the phenotype in two or more independent trials; "+/−" indicates that at least 50% of embryos exhibited the phenotype in two or more independent trials.

See Figure S1 for a similar phenotypic profile induced by a known TGF-β inhibitor, SB-505124.

K

	Phenotypic Profile			
Stage of exposure to Heterotaxin	Left-right asymmetry	Vasculogenesis/ Angiogenesis	Melanogenesis	Migration
10-46	+	+	+	+
12-46	+	+	+	+
18-46	+	+	+	+
26-46	+/-	+	+	+
32-46	-	+/-	+	+
10-26	+	-	-	-

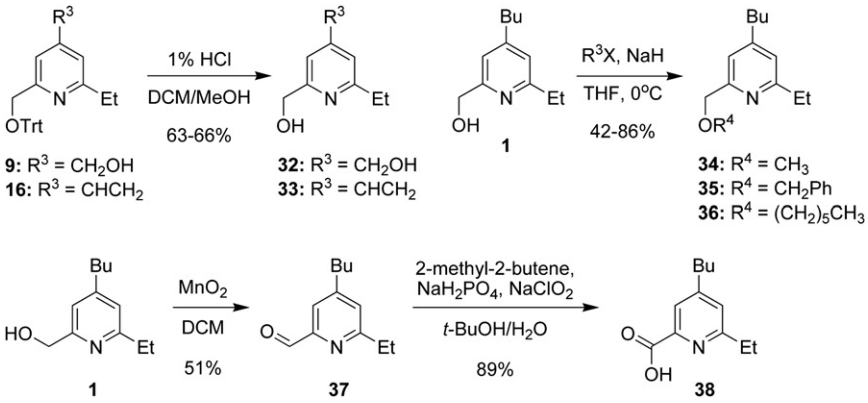

Figure 5. Synthesis of Additional Heterotaxin Analogs from Common Precursors
See Table S1 for SAR analyses of heterotaxin analogs and Supplemental Experimental Procedures.

the diyne **5** and a variety of different nitriles (propionitrile, valeronitrile, and benzonitrile), delivering the fused, regioisomerically pure pyridines **6–8** (R^1 = ethyl, butyl, phenyl) in 82%–98% yield. The silicon tether was then removed using TBAF to afford the 2,4,6-substituted pyridines **9–11** in 86%–99% yield. The alcohols **9–11** were converted into the aldehydes **12–14** in 84%–90% yield using the previously employed Swern oxidation, followed by a Wittig reaction with several different alkylphosphonium bromides to install different chain lengths at the four position in **15–20** (R^2 = methyl, propyl, butyl, pentyl). Reduction of the double bond in **15–20** with Pd/C under 1 atm of H_2 furnished the pyridines **21–26** in almost quantitative yields. The acid-catalyzed deprotection of the trityl group proceeded smoothly and delivered the heterotaxin analogs **27–31** in 71%–100% yield.

Two additional analogs were synthesized by deprotection of the trityl group at different stages of the synthesis (Figure 5). One deprotection was conducted after removal of the silicon tether from **9** to afford the diol **32** in 66% yield, and the second was performed on the alkene **16** to obtain the compound **33** in 63% yield. Installation of different hydrocarbon substituents on the hydroxyl group of heterotaxin (**1**) was accomplished by subjecting **1** to deprotonation with NaH, followed by the addition of the appropriate alkyl halide (methyl, benzyl, and hexyl) to afford the ethers **34–36** in 42%–86% yield. Finally, the hydroxyl group of heterotaxin (**1**) was oxidized to the carboxylic acid **38** by a two-step oxidation process. First, the aldehyde **37** was formed in moderate yield by oxidation of the alcohol **1** with MnO_2, followed by a Lindgren oxidation (Stangeland and Sammakia, 2004; Lindgren and Nilsson, 1973) to form the carboxylic acid **38** in 89% yield (Figure 5).

The length of the alkyl chain at the CH_2R^2 substituent was found to be critical for the specific activity of this class of molecules, with the highest activity being observed for butyl (heterotaxin, **1**) and pentyl (**28**), whereas ethyl (**27**), ethylene (**33**), hydroxymethylene (**32**), and hexyl (**29**) were inactive (or toxic) (see Table S1 available online). Although the size of the R^1 group does not appear to be critical, as ethyl (heterotaxin, **1**), butyl (**31**), and phenyl (**30**) are tolerated, both the butyl (**31**) and phenyl (**30**) substitutions did yield more potent analogs, which exhibited activity at lower concentrations than the original heterotaxin molecule (EC_{50} values = 10 and 50 μM, respectively) (Table S1). Furthermore, although modifications of the CH_2OH group through methylation (**34**), oxidation (**38**), or alkylation (**36**) did not have a major effect on activity, benzylation (**35**) produced a very active compound (EC_{50} value = 10 μM) (Table S1). Interestingly, for each analog, the EC_{50} for inducing defects in asymmetric organogenesis was identical to the EC_{50} for perturbing melanogenesis, vasculogenesis/angiogenesis, and/or gut elongation, although the severity of each phenotype varied between analogs (Table S1). These results show that replacing individual substituents does not isolate the various activities of the compound, suggesting that the individual phenotypes induced by heterotaxin are not chemically separable and may result from perturbation of the same biological target.

Identifying the Cellular Target of Heterotaxin Analogs

Our phenocritical timing studies suggest that heterotaxin perturbs left-right asymmetry during the stages when asymmetrically expressed TGF-β ligands, such as nodal, establish organ laterality. Therefore, we hypothesized that TGF-β signaling is inhibited by heterotaxin. Because the above SAR studies indicate that the various phenotypes induced by heterotaxin are not chemically separable, it is possible that the complete phenotypic profile of this compound is attributable to inhibited TGF-β signaling. This hypothesis is strongly supported by the fact that exposure to a known small molecule TGF-β signaling inhibitor, SB505124 (DaCosta Byfield et al., 2004), induced the same phenotypic profile as our compounds, including heterotaxia, vasculogenesis and melanogenesis defects, and aberrant migratory cell properties, within the same phenocritical periods (Figure S1). Importantly, other signaling pathways that also influence all four of these developmental processes are unaffected by heterotaxin (Figure S1).

To test the hypothesis that heterotaxin interferes with TGF-β signaling, we evaluated the expression of *Xantivin*, the *Xenopus* homolog of *lefty*, which is normally expressed in the left LPM as a direct consequence of nodal-type TGF-β signaling (Ho et al., 2006). Although DMSO-treated control embryos exhibit normal expression of this target gene in the left LPM, *Xantivin* could not be detected in the left or right LPM of heterotaxin-treated embryos (Figure 6A; Figure S2), strongly suggesting that nodal-type TGF-β signaling is inhibited by heterotaxin. These data are consistent with previous reports in which embryos exposed to a known TGF-β signaling inhibitor failed to express *Xantivin* (Ho et al., 2006).

TGF-β receptor activation is conveyed by the phosphorylation of intracellular mediators, known as Smads, which ultimately effect transcription (ten Dijke and Hill, 2004). Nodal signaling occurs primarily via phosphorylation of Smad2; thus, the level of phosphorylated Smad2 in *Xenopus* extracts may be used as an indicator of embryonic nodal-type TGF-β signaling

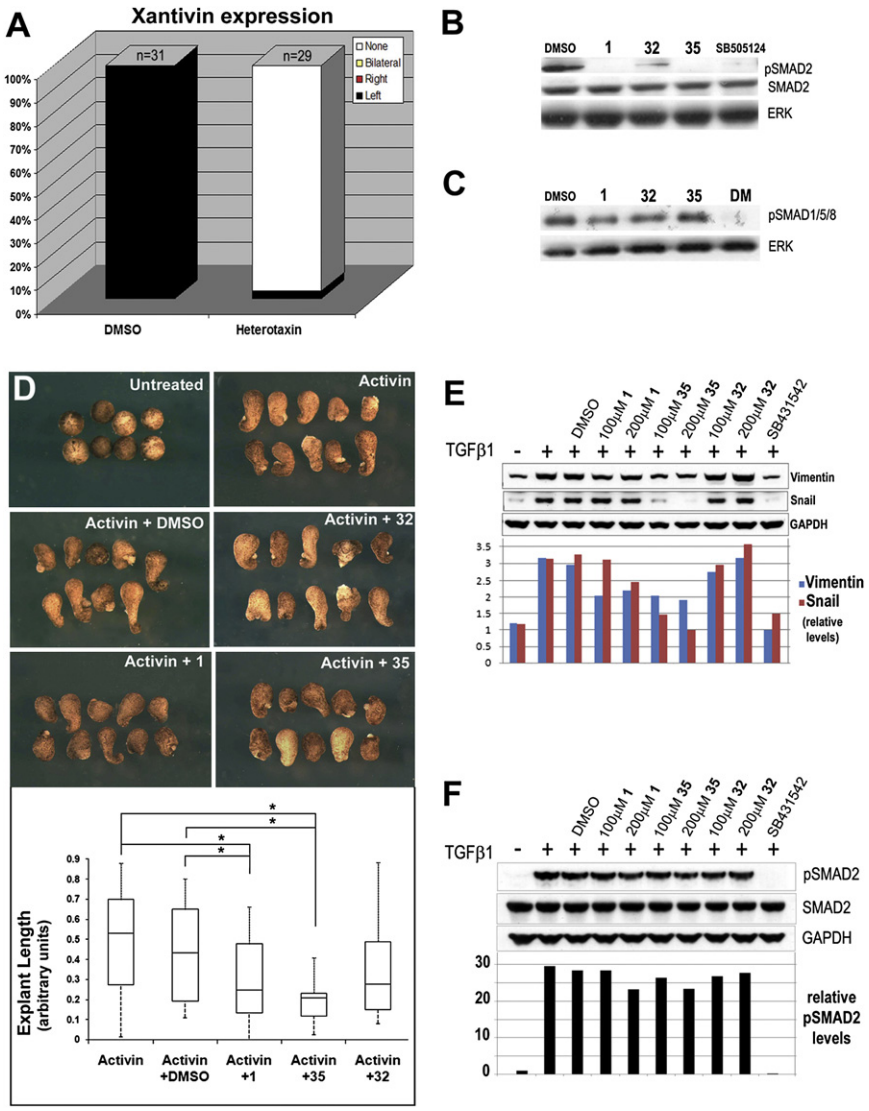

Figure 6. Heterotaxin Inhibits TGF-β Signaling

(A) The frequency of embryos exhibiting left only (Left, black), right only (Right, red), bilateral (gray), or absent (None, white) expression of *Xantivin* is quantified in the bar graphs. (See Figure S2 for images of in situ hybridization).

(B) Western blotting of embryos exposed from 10 hpf for 24 hr to DMSO, 200 μM heterotaxin (**1**), 200 μM phenotypically inactive analog (**32**), 80 μM active analog (**35**), and a known nodal signaling inhibitor (SB-505124; 50 μM). Although unmodified Smad2 is detected under all conditions, phosphorylated Smad2 (pSmad2) is only detected in the presence of DMSO or the inactive heterotaxin analog **32** (albeit at reduced levels). ERK is total protein control.

(C) Western blotting of embryos exposed to DMSO, **1, 32**, **35** and the BMP signaling inhibitor, dorsomorphin (DM; 50 μM). BMP-specific Smad1/4/5 levels are unaffected by heterotaxin analogs.

(D) Activin-induced elongation in *Xenopus* animal cap explants is inhibited by active heterotaxin analogs **1** and **35**, but not DMSO or analog **32**. The box plot shows that activin-induced lengthening (results pooled from two identical trials) is inhibited significantly only by compounds **1** and **35**, as calculated by one-way ANOVA (*$p < 0.05$). Error bars indicate the first through third interquartile range of the measured lengths.

(E) Western blotting of A549 cells exposed to 10 ng/ml TGF-β1 and DMSO, 100–200 μM **1, 32**, **35**, or 10 μM SB-431542 for 48 hr. TGF-β1-induced upregulation of Vimentin and Snail is inhibited by analogs **1** and **35**, but not DMSO or analog **32**. GAPDH is total protein control.

(F) Western blotting of A549 cells exposed to 10 ng/ml TGF-β1 and DMSO, 100–200 μM **1, 32**, **35**, or 10 μM SB-431542 for 1 hr. TGF-β1-induced phosphorylation of Smad2 is unaffected by heterotaxin analogs. GAPDH controls for total protein.

See Figure S2 for effect of **1** on non-Smad-dependent TGF-β signaling via PI3K/Akt.

(Ho et al., 2006). As expected, the level of phosphorylated Smad2 is unaffected by exposure to DMSO (Figure 6B, lane 1). However, Smad2 phosphorylation is abolished in embryos exposed to heterotaxin (**1**) (Figure 6B, lane 2), or to the more potent heterotaxin analog **35** (Figure 6B, lane 4), but is only mildly downregulated by exposure to the phenotypically inactive heterotaxin analog **32** (Figure 6B, lane 3). The inhibition of Smad2 phosphorylation by heterotaxin is comparable to that induced by SB-505124 (Figure 6B, lane 5). Importantly, the level of phosphorylated Smad1/5/8, which indicates signaling via other TGF-β superfamily ligands such as BMP, remains unaffected by heterotaxin analogs (Figure 6C); thus, the effect of heterotaxin is specific for Smad2-dependent TGF-β signaling.

A unique advantage of amphibian embryos is the ability to culture specific embryonic tissues ex vivo in order to isolate the effects of exogenous growth factors on cell behavior. It is well established that the addition of the Smad2-mediated TGF-β ligand activin to *Xenopus* "animal cap" explants can elicit concentration-dependent elongation in a tissue that would otherwise remain naive to TGF-β signals and fail to elongate at all (Green, 1999). We employed this assay to quantify the degree to which heterotaxin analogs interfere with TGF-β-ligand-dependent signaling. In contrast to DMSO or the inactive analog **32**, heterotaxin (**1**) and the potent analog **35** significantly inhibit activin-induced animal cap elongation (Figure 6D); thus, heterotaxin analogs inhibit activin-dependent activity in *Xenopus*.

To determine if heterotaxin analogs inhibit the activity of other TGF-β ligands, we assessed their activity in human cell culture. A549 cells undergo an epithelial-mesenchymal transition in response to TGF-β1 (Kim et al., 2007), as indicated by the upregulation of mesenchymal markers such as Snail and Vimentin (Figure 6E, compare lanes 1–2). Heterotaxin (**1**) and the potent analog **35** inhibit the upregulation of these markers (Figure 6E, lanes 4–7), whereas DMSO or the inactive analog **32** has no effect (Figure 6E, lanes 3 and 8–9); thus, heterotaxin analogs inhibit TGF-β1-dependent activity in human cells.

To determine if heterotaxin compounds directly affect ligand-dependent Smad2 phosphorylation, we assessed levels of

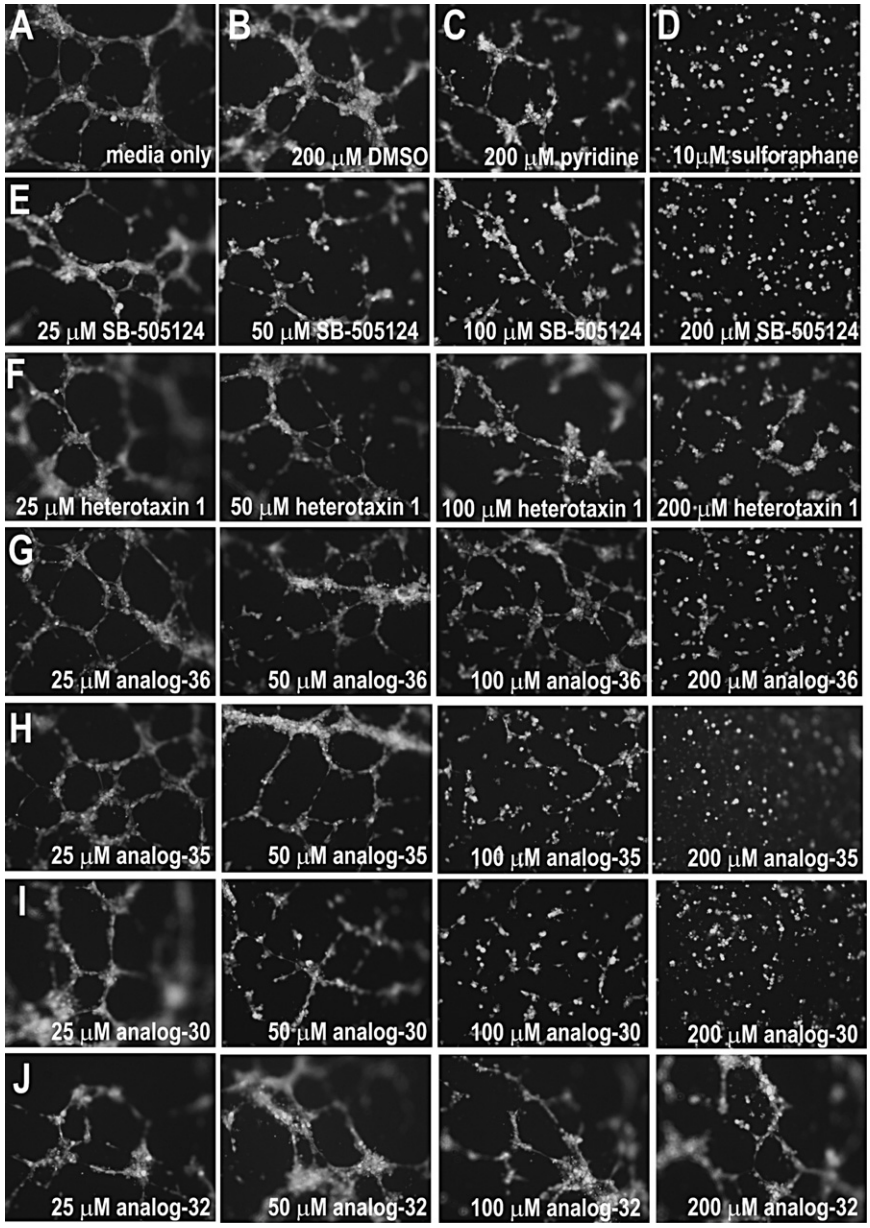

Figure 7. Heterotaxin Inhibits Angiogenesis in Human Cells

HUVECs form tubes when cultured in the presence of media alone (A), DMSO (B), unsubstituted pyridine (C), or the inactive heterotaxin analog **32** (J). In contrast, HUVECs cultured in the presence of a known anti-angiogenic agent, sulforaphane (D) (Bertl et al., 2006), are unable to form tubes. Although the original heterotaxin molecule **1** (F) exhibits only very mild anti-angiogenic effects in this assay (at 6 hr), the other active heterotaxin analogs **36** (G), **35** (H), and **30** (I) have obvious concentration-dependent anti-angiogenic properties comparable to a known TGF-β signaling inhibitor (E, SB-505124). Cells were stained with Calcein AM to confirm viability.

See Figure S3 for effect of analog **30** on tumor cell growth.

phosphorylated Smad2 in these cells with a 1-hr TGF-β1 induction (Figure 6F). Compared to the effect of SB431542, a known TGF-β type I receptor inhibitor (Inman et al., 2002), TGF-β1-induced Smad2 phosphorylation remained relatively unaffected by our compounds in this time frame, suggesting that the effect of heterotaxin on Smad2 phosphorylation in vivo may not involve direct inhibition of TGF-β receptors or may inhibit a non-Smad-dependent TGF-β signaling pathway (Zhang, 2009).

We tested the latter possibility by assessing the effect of heterotaxin on TGF-β1-induced activation of phosphatidylinositol 3-kinase (PI3K), as well as mitogen-activated protein kinases (MAPKs), including p38, c-Jun amino-terminal kinase (JNK), and extracellular signal-regulated kinase (ERK). Although the activation of most of these non-Smad pathways was not suppressed by our compound (data not shown), TGF-β1-induced activation of PI3K (1 hr induction), as indicated by the levels of phosphorylated Akt (Ser-473) (Figure S2E, lanes 1–2), was inhibited by heterotaxin (**1**) (Figure S2E, lanes 4–5), whereas DMSO and the inactive analog **32** had no effect (Figure S2E, lanes 3 and 6). Taken together, these results indicate that 2,4,6-substituted pyridines function as both indirect (Smad2 dependent) and direct (non-Smad dependent) TGF-β signaling inhibitors.

Heterotaxin Analogs Exhibit Anti-Angiogenic Properties in Mammalian Cells

In addition to development, the TGF-β pathway also plays a multiphasic role in tumor progression. Although early in tumorigenesis TGF-β is tumor suppressive (Jakowlew, 2006), later tumor cells are resistant to TGF-β-mediated growth inhibition, and upregulation of TGF-β facilitates metastatic invasion, promoting cell migration and epithelial-to-mesenchymal transition (Yingling et al., 2004; Tian et al., 2003), as well as new blood vessel growth and angiogenesis (ten Dijke and Arthur, 2007), crucial requirements for tumor growth and metastasis.

Therefore, TGF-β signaling inhibitors, like heterotaxin and its analogs, may be useful for blocking the tumor-promoting effects of TGF-β. Because our compounds inhibit vascular development in vivo, we assessed their anti-angiogenic potential in a mammalian system (Figure 7). The human umbilical vein endothelial cell (HUVEC) assay provides a visual readout of the ability of exogenous factors to inhibit the formation of microcapillary tubes (e.g., Figure 7D). Compared to solvent or pyridine controls (Figures 7B and 7C), the heterotaxin analogs that inhibited vascular development in *Xenopus* (e.g., **1**, **30**, **35**, **36**) (see Table S1) were also able to inhibit tube formation (Figures 7F–7I) in HUVEC cultures.

The effects were comparable to those elicited by a known TGF-β receptor inhibitor (Figure 7E). However, whereas TGF-β receptor inhibitors can also block the growth-inhibitory effects of TGF-β (e.g., SB-431542; Halder et al. [2005]), promoting tumorigenesis, heterotaxin analogs appear not to have this limitation. In fact, compound **30** not only inhibits angiogenesis (Figure 7I) but also significantly inhibits growth in several mammalian tumor cell lines (Figure S3). Thus, 2,4,6-substituted pyridine analogs may be broadly applicable in the development of anti-angiogenic antitumor compounds in mammalian systems.

DISCUSSION

A multi-phenotype-based whole organism screen of small molecules in *X. laevis* embryos identified a novel class of pyridines with TGF-β inhibitory activity. Our data have implications for understanding the role of the TGF-β pathway in the development of left-right asymmetry, gut morphogenesis, melanogenesis, and vascular development, and for the employment of heterotaxin analogs in the development of TGF-β inhibitory lead compounds with therapeutic potential.

Heterotaxin and the Role of TGF-β in Left-Right Asymmetry, Melanogenesis, Vasculogenesis, and Gut Development

Our results validate our phenotypic screen for heterotaxia because TGF-β ligands are well known to play an evolutionarily conserved role in the development of left-right asymmetry (Whitman and Mercola, 2001). Moreover, in addition to left-right patterning, TGF-β signaling has also been implicated in the other biological processes disrupted by heterotaxin. For example, TGF-β signaling is required for the assembly of the embryonic vasculature (ten Dijke and Arthur, 2007), the establishment of vessel wall integrity (Pepper, 1997), and the regulation of vascular homeostasis (Bertolino et al., 2005). As might be predicted to occur in the presence of a TGF-β inhibitor, heterotaxin dramatically impairs angiogenesis both in vivo and in vitro. Because in vitro tube formation may also be influenced by other factors, confirmation of a direct effect of heterotaxin on human angiogenesis must await further studies in mammalian models. Nonetheless, the similarity of the anti-angiogenic activity profiles of heterotaxin analogs in both frog embryos and human cells suggests that these compounds could have broader applicability.

In addition, TGF-β signaling normally increases melanocyte precursor proliferation (Kawakami et al., 2002) but inhibits melanogenic differentiation (Kim et al., 2004). Consistent with the expected outcome of inhibiting TGF-β signaling, heterotaxin exposure during melanocyte precursor migration and differentiation results in decreased melanocyte number but increased dendricity. Because *nodal* is expressed in aggressive melanomas, which reacquire melanocyte precursor-like properties, heterotaxin analogs may be promising in the development of differentiation-based anti-melanoma therapies (Hendrix et al., 2007).

Finally, in multiple contexts, TGF-β signaling induces cell motility and decreased E-cadherin-mediated intercellular adhesion in cells undergoing epithelial-to-mesenchymal transitions (Xu et al., 2009). In the developing gut, heterotaxin inhibits migratory cell morphology and behavior, and concomitantly increases E-cadherin levels, as might be predicted for an inhibitor of TGF-β signaling. The effect of heterotaxin on gut morphogenesis provides a novel inroad for investigating the role of TGF-β signaling in the poorly understood processes of gut elongation and rotation.

The Cellular Target of Heterotaxin

Heterotaxin compounds disrupt Smad2 phosphorylation in vivo, although this is not a direct effect. Possible mechanisms of action of heterotaxin and its analogs include inhibiting the synthesis, secretion, or processing of TGF-β receptors or ligands. Alternatively, these compounds could be influencing non-Smad-dependent pathways downstream of TGF-β receptors. Indeed, we found that heterotaxin directly inhibits TGF-β-induced PI3K activity. Although activation of PI3K by TGF-β requires the activity of TGF-β receptors, the molecular interactions underlying the activation of non-Smad-dependent TGF-β signaling events are extremely complex and context dependent (Zhang, 2009). Therefore, further investigations of the role of PI3K-mediated TGF-β signaling during *Xenopus* development will be required before the cellular target(s) of 2,4,6-substituted pyridines can be fully resolved. Nonetheless, because non-Smad-dependent TGF-β pathways are frequently involved in activating the pro-oncogenic effects of TGF-β signaling during tumor progression, e.g., PI3K-Akt signaling is required for Smad-dependent transcriptional responses as well as tumor cell migration (Bakin et al., 2000), our results raise the exciting possibility that heterotaxin compounds might be able to selectively target TGF-β-dependent tumor-promoting outcomes without also blocking the tumor-suppressive effects of TGF-β. This property could be important for selectively controlling distinct TGF-β responses in different therapeutic contexts.

Heterotaxin Analogs as Therapeutic Agents

Because of their important roles in tumorigenesis, TGF-β pathway components are excellent chemotherapeutic targets, although compounds that can appropriately modulate this multifunctional pathway in vivo are still in development. We discovered compounds that specifically inhibit *nodal*-dependent gene expression and multiple TGF-β-dependent biological processes in a whole vertebrate embryo, including neovascularization and migratory behavior. In addition, heterotaxin analogs inhibit TGF-β-induced epithelial-mesenchymal transition and angiogenesis in human cells, while inhibiting the growth of multiple mammalian tumor cell lines. Thus, heterotaxin analogs exhibit highly desirable biological activity and may be valuable in the development of TGF-β-inhibitory chemotherapeutics for blocking tumor proliferation and/or metastasis.

SIGNIFICANCE

In the developing embryo, a myriad of cellular processes form organs in a dynamic and complex three-dimensional milieu. In disease states these same processes occur inappropriately in equally complicated adult environments. Identifying small molecules that can predictably modulate cellular processes in their multifarious biological contexts is imperative for the discovery of effective drugs and stem

cell therapies. However, many lead compounds are initially identified in target-based biochemical or simplified cell-based assays because such assays are amenable to high-throughput screening; consequently, the in vivo effects of such compounds are often unpredictable. Although multiplexed profiling can provide important information about potential toxicity and mechanism of action, such knowledge is not necessarily predictive of efficacy in vivo. Moreover, even when a compound has been identified in a whole organism phenotype-based screen, there is as yet, to our knowledge, no reliable or systematic way to determine its cellular target(s).

We have shown that a whole organism multi-phenotype profiling strategy can be used to both identify compounds capable of modulating important biological processes in vivo *and* to infer mechanism of action. Using a combination of independent tissue-level developmental phenotypes, immunohistochemical analyses, gene expression patterns, tissue culture, and biochemical assays, we discovered a class of TGF-β signaling inhibitors. Remarkably, these compounds also elicit TGF-β-dependent phenotypes in human cells that mirror their activity profiles in vivo, suggesting that they may be valuable in the development of therapeutic agents to inhibit pathologic conditions mediated by excess TGF-β signaling (e.g., metastasis, fibrosis). Our discovery suggests that multi-phenotype profiling in whole organisms is a powerful strategy for identifying the pathway-level mechanism of action of small molecules.

EXPERIMENTAL PROCEDURES

Embryo Screening and Animal Caps

Experiments involving live animals were performed in accordance with national regulations, and approved by the NC State University Institutional Animal Care and Use Committee. *X. laevis* embryos were obtained by in vitro fertilization, de-jellied with 2% cysteine-HCl (pH 7.8–8.1), sorted to eliminate anomalous individuals, and cultured in 0.1× MMR at 15°C–22°C (Sive et al., 1998). Staging was according to Nieuwkoop and Faber (1994).

Stock solutions were prepared in DMSO (20 mM). For the screen, approximately 130 compounds were diluted to 200 μM in 2 ml 0.1× MMR in a 24-well plate; 1% DMSO was used as a solvent control. Four embryos were exposed in each well starting at ~10 hr after fertilization. Organs were evaluated in anesthetized tadpoles (0.05% MS-222) when controls reached stage 44–46.

Animal caps were dissected (Green, 1999) and cultured in 5 ng/ml human activin A (R&D Systems), or activin plus DMSO, 200 μM **1**, **32**, or **35** for 2 hr. Caps were then cultured 8 hr in 0.75× MMR + gentamycin (Sive et al., 1998). Final explant lengths were calculated using Photoshop CS2 (Measure tool). The significance of decreased elongation was determined by one-way ANOVA between groups.

In Situ Hybridization and Immunohistochemistry

Embryos were fixed at st 23/26 in MEMFA (Sive et al., 1998). Digoxigenin-labeled riboprobes for *Xnr-1*, *Xantivin* (gift of C. Wright), and *XPitx2c* were synthesized from linearized plasmids (Muller et al., 2003). In situ hybridization was as described (Lipscomb et al., 2006). St 44 embryos were fixed for immunohistochemistry and processed for cryosectioning (Fagotto and Gumbiner, 1994). Staining was performed using anti-E-cadherin (DSHB; 5D3 at 1:200) and anti-laminin (Sigma; L9393 at 1:200) primary antibodies and Alexa-conjugated secondary antibodies (Invitrogen; 1:2000), as described (Reed et al., 2009).

Tube Formation

HUVECs were cultured in Media 200PRF with LSGS supplement (Invitrogen). The Cultrex® In Vitro Angiogenesis Assay Tube Formation Kit (Trevigen) was used according to manufacturer's protocol. Subconfluent HUVECs at passage 5 (~80% confluent) were incubated with 2 μM Calcein AM for 30 min at 37°C to allow for fluorescent monitoring of cell viability and tube formation. Cells were treated with DMSO, sulforaphane, or heterotaxin analogs/SB-505124 at the time of seeding. Tube formation was assessed 6 hr after treatment.

Western Blotting

St 10 embryos were exposed to DMSO, heterotaxin analogs, SB-505124, or dorsomorphin for 24 hr. Ten embryos from each treatment were pelleted, resuspended in 100 μl lysis buffer (20 mM Tris [pH 7.4], 150 mM NaCl, 1 mM EDTA, 1 mM EGTA, 1% Triton, 2.5 mM sodium pyrophosphate, 1 mM b-glycerophosphate, 1 mM sodium vanadate, 1 μg/ml leupeptin), and lysed by mechanical disruption, followed by freeze-thaw cycles. Approximately 20 μg of each cleared lysate was run on a 10% NuPAGE Bis-Tris gel and then transferred to a PVDF membrane. Membranes were blocked for 1 hr in TBST (20 mM Tris [pH 7.6], 136 mM NaCl, 0.1% Tween 20) + 5% nonfat dry milk, and incubated overnight at 4°C with primary antibodies (see below). Membranes were washed four times in TBST, incubated for 2 hr in TBST+ 5% nonfat dry milk and HRP-conjugated donkey anti-rabbit IgG (Upstate), washed three to four times in TBST, then visualized using chemiluminescence with SuperSignal West Pico (Pierce).

A549 cells (ATCC) were maintained in DMEM with antibiotics and 10% FBS. Cells were starved overnight in DMEM with 1% FBS and incubated with DMSO, heterotaxin analogs, or SB-431542 in DMEM with 10% FBS for 30 min before treatment with rhTGFβ1 (R&D Systems) for 1–48 hr. Whole-cell lysates were prepared in RIPA lysis buffer (Pierce) with complete Mini EDTA Protease Inhibitor and Phos-STOP (Roche) and sonication. Approximately 40 μg of each cleared lysate was run on a 4%–12% NuPAGE Bis-Tris gel and then transferred to a nitrocellulose membrane before blocking and antibody staining as above. Autoradiography bands were scanned and quantitated with ImageJ freeware. The integrated optical density of each band was normalized to GAPDH or β-actin and the fold change determined by dividing each normalized value by the lowest normalized sample value.

Primary antibodies used were Smad2, phospho-Smad2, phospho-Smad1/5/8, phospho-p38, Erk, phospho-Erk, phospho-SAPK/JNK, phospho-Akt (Ser473), and Snail from Cell Signaling Technology, and Vimentin, β-actin, and GAPDH from Santa Cruz Biotechnology.

SUPPLEMENTAL INFORMATION

Supplemental Information includes Supplemental Experimental Procedures, three figures, and one table and can be found with this article online at doi:10.1016/j.chembiol.2010.12.008.

ACKNOWLEDGMENTS

We thank Dr. K. Symes for experimental advice and Brooke Griff for technical assistance. This work was supported by NSF (IOB 0642012; NNY), NIH (RO1 DK085300-01A1; NNY), and NCSU CCMTR (NNY, AD, MLH). A.D. is a recipient of an NSF CAREER Award (CHE 0846756).

Received: January 20, 2010
Revised: December 3, 2010
Accepted: December 5, 2010
Published: February 24, 2011

REFERENCES

Adams, D.S., Robinson, K.R., Fukumoto, T., Yuan, S., Albertson, R.C., Yelick, P., Kuo, L., McSweeney, M., and Levin, M. (2006). Early, H+-V-ATPase-dependent proton flux is necessary for consistent left-right patterning of non-mammalian vertebrates. Development *133*, 1657–1671.

Bakin, A.V., Tomlinson, A.K., Bhowmick, N.A., Moses, H.L., and Arteaga, C.L. (2000). Phosphatidylinositol 3-kinase function is required for transforming growth factor beta-mediated epithelial to mesenchymal transition and cell migration. J. Biol. Chem. *275*, 36803–36810.

Bertl, E., Bartsch, H., and Gerhauser, C. (2006). Inhibition of angiogenesis and endothelial cell functions are novel sulforaphane-mediated mechanisms in chemoprevention. Mol. Cancer Ther. *5*, 575–585.

Bertolino, P., Deckers, M., Lebrin, F., and ten Dijke, P. (2005). Transforming growth factor-beta signal transduction in angiogenesis and vascular disorders. Chest *128*, 585S–590S.

Bols, M., and Skrydstrup, T. (1995). Silicon-tethered reactions. Chem. Rev. *95*, 1253–1277.

Brueckner, M. (2007). Heterotaxia, congenital heart disease, and primary ciliary dyskinesia. Circulation *115*, 2793–2795.

Collazo, A., Bronner-Fraser, M., and Fraser, S.E. (1993). Vital dye labelling of *Xenopus laevis* trunk neural crest reveals multipotency and novel pathways of migration. Development *118*, 363–376.

DaCosta Byfield, S., Major, C., Laping, N.J., and Roberts, A.B. (2004). SB-505124 is a selective inhibitor of transforming growth factor-beta type I receptors ALK4, ALK5, and ALK7. Mol. Pharmacol. *65*, 744–752.

Fagotto, F., and Gumbiner, B.M. (1994). Beta-catenin localization during *Xenopus* embryogenesis: accumulation at tissue and somite boundaries. Development *120*, 3667–3679.

Feng, Y., Mitchison, T.J., Bender, A., Young, D.W., and Tallarico, J.A. (2009). Multi-parameter phenotypic profiling: using cellular effects to characterize small-molecule compounds. Nat. Rev. Drug Discov. *8*, 567–578.

Green, J. (1999). The animal cap assay. Methods Mol. Biol. *127*, 1–13.

Halder, S.K., Beauchamp, R.D., and Datta, P.K. (2005). A specific inhibitor of TGF-beta receptor kinase, SB-431542, as a potent antitumor agent for human cancers. Neoplasia *7*, 509–521.

Hendrix, M.J., Seftor, E.A., Seftor, R.E., Kasemeier-Kulesa, J., Kulesa, P.M., and Postovit, L.M. (2007). Reprogramming metastatic tumour cells with embryonic microenvironments. Nat. Rev. Cancer *7*, 246–255.

Ho, D.M., Chan, J., Bayliss, P., and Whitman, M. (2006). Inhibitor-resistant type I receptors reveal specific requirements for TGF-beta signaling in vivo. Dev. Biol. *295*, 730–742.

Inman, G.J., Nicolas, F.J., Callahan, J.F., Harling, J.D., Gaster, L.M., Reith, A.D., Laping, N.J., and Hill, C.S. (2002). SB-431542 is a potent and specific inhibitor of transforming growth factor-beta superfamily type I activin receptor-like kinase (ALK) receptors ALK4, ALK5, and ALK7. Mol. Pharmacol. *62*, 65–74.

Inui, M., and Asashima, M. (2006). A novel gene, Ami is expressed in vascular tissue in *Xenopus laevis*. Gene Expr. Patterns *6*, 613–619.

Jakowlew, S.B. (2006). Transforming growth factor-beta in cancer and metastasis. Cancer Metastasis Rev. *25*, 435–457.

Kamal, I.M. (2000). Defusing the intra-abdominal ticking bomb: intestinal malrotation in children. CMAJ *162*, 1315–1317.

Kawakami, T., Soma, Y., Kawa, Y., Ito, M., Yamasaki, E., Watabe, H., Hosaka, E., Yajima, K., Ohsumi, K., and Mizoguchi, M. (2002). Transforming growth factor beta1 regulates melanocyte proliferation and differentiation in mouse neural crest cells via stem cell factor/KIT signaling. J. Invest. Dermatol. *118*, 471–478.

Kim, D.S., Park, S.H., and Park, K.C. (2004). Transforming growth factor-beta1 decreases melanin synthesis via delayed extracellular signal-regulated kinase activation. Int. J. Biochem. Cell Biol. *36*, 1482–1491.

Kim, J.H., Jang, Y.S., Eom, K.S., Hwang, Y.I., Kang, H.R., Jang, S.H., Kim, C.H., Park, Y.B., Lee, M.G., Hyun, I.G., et al. (2007). Transforming growth factor beta1 induces epithelial-to-mesenchymal transition of A549 cells. J. Korean Med. Sci. *22*, 898–904.

Levin, M. (2005). Left-right asymmetry in embryonic development: a comprehensive review. Mech. Dev. *122*, 3–25.

Lindgren, B.O., and Nilsson, T. (1973). Preparation of carboxylic-acids from aldehydes (including hydrolated benzaldehydes) by oxidation with chlorite. Acta Chem. Scand. *27*, 888–890.

Lipscomb, K., Schmitt, C., Sablyak, A., Yoder, J.A., and Nascone-Yoder, N. (2006). Role for retinoid signaling in left-right asymmetric digestive organ morphogenesis. Dev. Dyn. *235*, 2266–2275.

Muller, J.K., Prather, D.R., and Nascone-Yoder, N.M. (2003). Left-right asymmetric morphogenesis in the *Xenopus* digestive system. Dev. Dyn. *228*, 672–682.

Nieuwkoop, P.D., and Faber, J. (1994). Normal Table of *Xenopus laevis* (Daudin) (New York: Garland Publishing Inc).

Ohi, Y., and Wright, C.V. (2007). Anteriorward shifting of asymmetric Xnr1 expression and contralateral communication in left-right specification in *Xenopus*. Dev. Biol. *301*, 447–463.

Pepper, M.S. (1997). Transforming growth factor-beta: vasculogenesis, angiogenesis, and vessel wall integrity. Cytokine Growth Factor Rev. *8*, 21–43.

Petit, M., Chouraqui, G., Aubert, C., and Malacria, M. (2003). New and efficient procedure for the preparation of unsymmetrical silaketals. Org. Lett. *5*, 2037–2040.

Reed, R.A., Womble, M.A., Dush, M.K., Tull, R.R., Bloom, S.K., Morckel, A.R., Devlin, E.W., and Nascone-Yoder, N.M. (2009). The morphogenesis of the primitive gut tube is generated by Rho/ROCK/Myosin II-mediated endoderm rearrangements. Dev. Dyn. *238*, 3111–3125.

Sive, H.L., Grainger, R.M., and Harland, R.M. (1998). Early Development of *Xenopus laevis* (Cold Spring Harbor, New York: Cold Spring Harbor Laboratory Press).

Stangeland, E.L., and Sammakia, T. (2004). Use of thiazoles in the halogen dance reaction: application to the total synthesis of WS75624 B. J. Org. Chem. *69*, 2381–2385.

ten Dijke, P., and Hill, C.S. (2004). New insights into TGF-beta-Smad signalling. Trends Biochem. Sci. *29*, 265–273.

ten Dijke, P., and Arthur, H.M. (2007). Extracellular control of TGFbeta signalling in vascular development and disease. Nat. Rev. Mol. Cell Biol. *8*, 857–869.

Tian, F., DaCosta Byfield, S., Parks, W.T., Yoo, S., Felici, A., Tang, B., Piek, E., Wakefield, L.M., and Roberts, A.B. (2003). Reduction in Smad2/3 signaling enhances tumorigenesis but suppresses metastasis of breast cancer cell lines. Cancer Res. *63*, 8284–8292.

Tomlinson, M.L., Guan, P., Morris, R.J., Fidock, M.D., Rejzek, M., Garcia-Morales, C., Field, R.A., and Wheeler, G.N. (2009). A chemical genomic approach identifies matrix metalloproteinases as playing an essential and specific role in *Xenopus* melanophore migration. Chem. Biol. *16*, 93–104.

Walmsley, M., Ciau-Uitz, A., and Patient, R. (2002). Adult and embryonic blood and endothelium derive from distinct precursor populations which are differentially programmed by BMP in *Xenopus*. Development *129*, 5683–5695.

Whitman, M., and Mercola, M. (2001). TGF-beta superfamily signaling and left-right asymmetry. Sci. STKE *2001*, re1.

Xu, J., Lamouille, S., and Derynck, R. (2009). TGF-beta-induced epithelial to mesenchymal transition. Cell Res. *19*, 156–172.

Yingling, J.M., Blanchard, K.L., and Sawyer, J.S. (2004). Development of TGF-beta signalling inhibitors for cancer therapy. Nat. Rev. Drug Discov. *3*, 1011–1022.

Young, D.D., Sripada, L., and Deiters, A. (2007). Microwave-assisted solid-supported alkyne cyclotrimerization reactions for combinatorial chemistry. J. Comb. Chem. *9*, 735–738.

Zhang, Y.E. (2009). Non-Smad pathways in TGF-beta signaling. Cell Res. *19*, 128–139.

Zhu, L., Belmont, J.W., and Ware, S.M. (2006). Genetics of human heterotaxias. Eur. J. Hum. Genet. *14*, 17–25.